ACS APPLIED MATERIALS & INTERFACES

Research Article

www.acsami.org

Giant Magnetoresistance and Anomalous Magnetic Properties of Highly Epitaxial Ferromagnetic $LaBaCo_2O_{5.5+\delta}$ Thin Films on (001) MgO

Ming Liu,[†,‡] Chunrui Ma,[‡] Jian Liu,[‡] Gregory Collins,[‡] Chonglin Chen,*[,‡] Jie He,[§] Jiechao Jiang,[§] Efstathios I. Meletis,[§] Li Sun,[#] Allan J. Jacobson,[¶] and Myung-Hwan Whangbo[▽]

[†]Electronic Materials Research Laboratory, Key Laboratory of the Ministry of Education & International Center for Dielectric Research, Xi'an Jiaotong University, Xi'an 710049, People's Republic of China

[‡]Department of Physics and Astronomy, University of Texas at San Antonio, Texas 78249, United States

[§]Department of Materials Science and Engineering, University of Texas at Arlington, Arlington, Texas 76019, United States

[#]Department of Mechanical Engineering, University of Houston, Houston, Texas 77204, United States

[¶]The Texas Center for Superconductivity and Department of Chemistry, University of Houston, Houston, Texas 77204, United States

[▽]Department of Chemistry, North Carolina State University, Raleigh, North Carolina 27695-8204, United States

ABSTRACT: Ferromagnetic thin films of the A-site nano-ordered double perovskite $LaBaCo_2O_{5.5+\delta}$ (LBCO) were grown on (001) MgO, and their structural and magnetic properties were characterized. The as-grown films have an excellent epitaxial behavior with atomically sharp interfaces, with the *c*-axis of the LBCO structure lying in the film plane and the interface relationship given by $(100)_{LBCO}//(001)_{MgO}$ and $[001]_{LBCO}//[100]_{MgO}$ or $[010]_{MgO}$. The as-grown LBCO films exhibit a giant magnetoresistance (54% at 40 K under 7 T) and an anomalous magnetic hysteresis, depending strongly on the temperature and the applied magnetic field scan width.

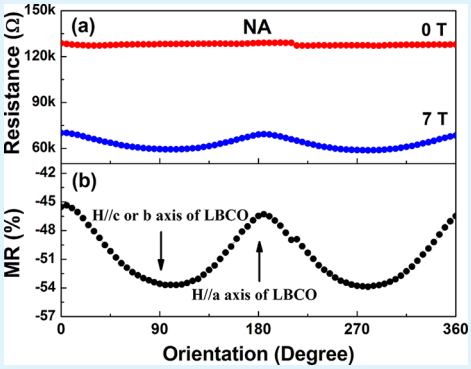

KEYWORDS: *$LaBaCo_2O_{5.5+\delta}$, interface, magnetoresistance, magnetic properties*

INTRODUCTION

Complex transition-metal oxides exhibit a wide range of electrical transport, magnetic, and optical properties that are scientifically interesting and technologically important. They have led to new physical phenomena such as negative thermal expansion,[1] spin valve effect,[2] and colossal magnetoresistance (MR) effect.[3] Multifunctional oxides are particularly interesting because they can be used for the development of various new nanodevices. Perovskite oxides with mixed ionic/electronic conductivity have useful applications in areas such as separation membranes, catalysts, sensitive gas sensors, and cathodes for solid oxide fuel cells.[4−7] Perovskite cobaltates exhibit remarkable mixed conductivity and catalytic properties at high temperature, as well as interesting magnetic and electrical transport properties at low temperature.[8,9] In particular, the oxygen-deficient double perovskite cobaltates $RACo_2O_{5.5+\delta}$ (R = rare earth and A = alkaline-earth) have received much attention.[10−14] Except for $LaBaCo_2O_{5.5+\delta}$ (LBCO), the $RBaCo_2O_{5.5+\delta}$ series form ordered structures under typical synthesis conditions in air. LBCO synthesized in air has a disordered arrangement of the cations but can be converted to an A-site ordered oxygen-deficient phase by heat treatment under argon at 1423 K.[15−18] In fully understanding the magnetic and transport properties of such complex cobalt oxides, the preparation of their single-crystalline samples is needed. To avoid the effects arising from the porosity and grain boundaries of polycrystalline samples, it is desirable to prepare highly epitaxial single-crystalline thin films on suitable substrates.

Recently, highly epitaxial single-crystalline thin films of LBCO were fabricated on (001) $LaAlO_3$[19,20] and (001) $SrTiO_3$,[21] and these films were found to possess an extraordinary sensitivity to reducing/oxidizing environments and an exceedingly fast redox reaction at high temperature. Furthermore, at low temperatures, the highly epitaxial LBCO thin films grown on (001) $SrTiO_3$ exhibit a large MR (19% at 40 K), which is much greater than expected from various phases of its bulk material. In this article, we show that highly

Received: July 23, 2012
Accepted: September 10, 2012
Published: September 10, 2012

   dx.doi.org/10.1021/am301427c | *ACS Appl. Mater. Interfaces* 2012, 4, 5524−5528

epitaxial LBCO films can be grown on (001) MgO, and these films have an unusually high MR of 54% and exhibit an anomalous magnetic behavior in both hysteresis and magnetic field scans. Especially, these properties depend sensitively on the temperature, the oxygen annealing, and the width of the magnetic field scan.

EXPERIMENTAL SECTION

The LBCO thin films were grown on (001) MgO using a KrF excimer pulsed-laser deposition system with a wavelength of 248 nm. Optimal growth was achieved at 850 °C under an oxygen pressure of 250 mTorr with a laser energy density of 2.0 J/cm^2. The LBCO thin films were annealed at 850 °C for 15 min in pure oxygen (200 Torr) before slowly cooling them down to room temperature at the rate of 5 °C/min. A group of the as-grown films were also annealed at 465 °C in a tube furnace under pure oxygen (1 atm) for 5 h to examine the effect of oxygen concentration on the film properties. The microstructure, crystallinity, and epitaxial behavior of the as-grown thin films were characterized by X-ray diffraction (XRD) and transmission electron microscopy (TEM). The electrical transport and magnetic properties of the LBCO films were systematically studied using a Quantum Design physical property measurement system.

RESULTS AND DISCUSSIONS

Microstructure Characterizations Using XRD and TEM. The crystalline quality of the LBCO films was examined by the XRD $\theta-2\theta$ scan, rocking curving, and ϕ scan measurements. All the films have a preferential a-axis orientation. Figure 1 shows results of a typical $\theta-2\theta$ scan for

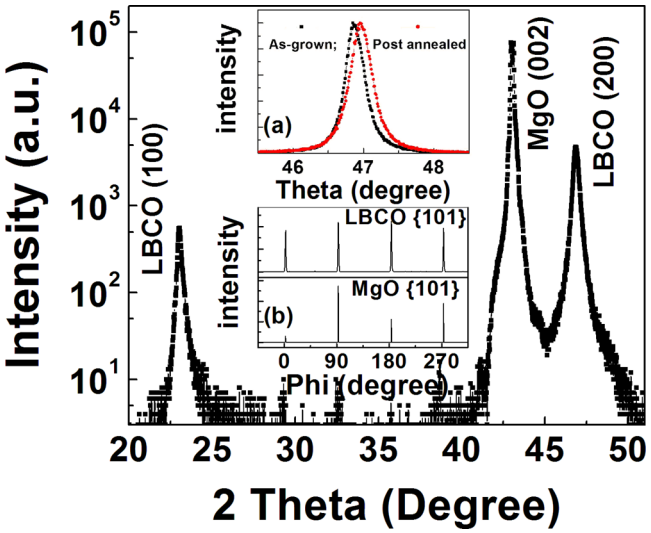

Figure 1. Typical XRD pattern of the as-grown LBCO films on (001) MgO substrates, which shows only the (h00) peaks in the diffraction scan. Inset (a) shows the (200) diffraction peaks of the as-grown and the oxygen-annealed films. Inset (b) shows the ϕ scans taken around the (101) diffraction of the LBCO films and MgO substrates, displaying that the films possess excellent epitaxial character.

the LBCO films on (001) MgO. Only the (h00) peaks appear in the $\theta-2\theta$ scans for both the LBCO films and the substrates, revealing that the films are highly oriented with the a-axis normal to the substrate surface. The XRD data for the films before and after oxygen annealing differ only in that the peak positions are shifted slightly to a higher angle by the annealing (for example, see the inset (a) of Figure 1 for the (200) diffraction peak). The latter suggests that the lattice parameter along the a-axis become smaller in the annealed films. Results of the ϕ scans, presented in the inset (b) of Figure 1, reveal only the (101) diffraction peaks of the films and those from the MgO substrates. The 4-fold symmetry and sharp peaks in the ϕ scan pattern suggest that the as-grown LBCO film have good single crystallinity. Therefore, the in-plane interface relationship of the films and the substrates is determined to be $[001]_{LBCO}//[100]_{MgO}$ and $(100)_{LBCO}//(001)_{MgO}$ from the ϕ scans, giving a very large lattice misfit value of ~7.5% (estimated from the peak positions of the films and the substrate). Furthermore, no significant difference was found before and after the annealing under pure oxygen.

The epitaxial behavior and interface microstructure of the LBCO films on (001) MgO were investigated by cross-sectional TEM measurements. A low-magnification bright-field TEM image of the LBCO film annealed in oxygen, presented in Figure 2a, shows that the film has an atomically sharp interface and an extremely smooth surface. Figures 2b and 2c show selected area electron diffraction (SAED) patterns, taken along the [010] MgO direction, of the LBCO film and the interface covering both the films and the substrate, respectively. The

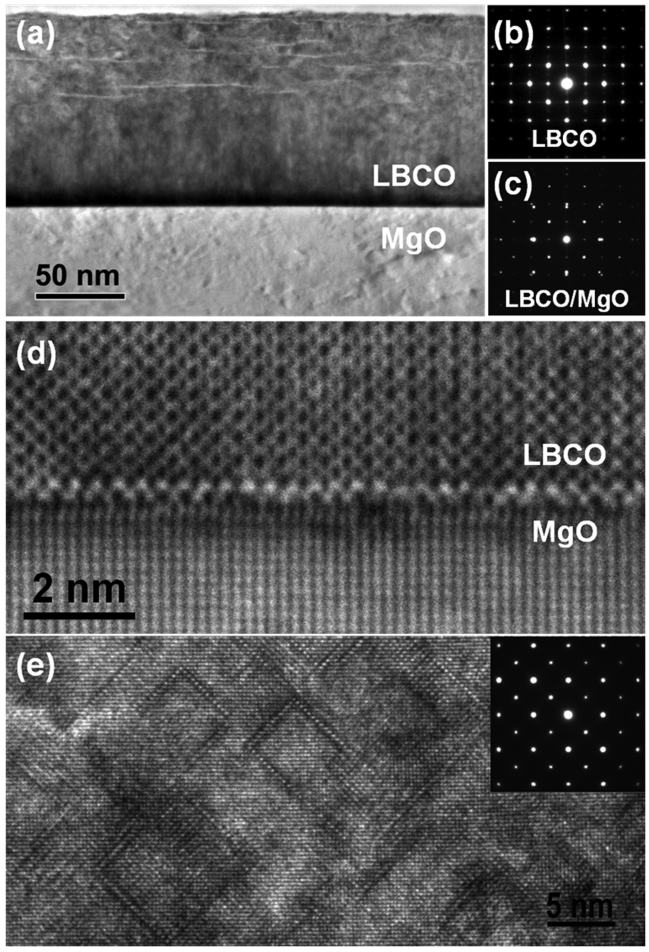

Figure 2. TEM images and SAED patterns of the oxygen-annealed LBCO films on (001) MgO substrate: (a) cross-sectional TEM image showing the epitaxial behavior and interface microstructure of the LBCO film, (b) SAED pattern from the LBCO film, (c) SAED pattern from the interface covering both the LBCO film and the MgO substrate, (d) high-resolution electron microscopy (HREM) image of the LBCO film showing the interface structure and epitaxial behavior, and (e) plan-view HREM image of a LBCO film exhibiting orthogonal nanodomains.

dx.doi.org/10.1021/am301427c | ACS Appl. Mater. Interfaces 2012, 4, 5524−5528

sharp electron diffraction spots with no satellites or broadening indicate that the films have good single crystallinity, which is in good agreement with the results from XRD scans. However, a careful examination of the diffraction pattern showed a set of weak diffraction spots located at the midpoints between two adjacent strong spots, indicating the formation of the 112-type ordered tetragonal structure in the LBCO films.[21,22] The *c*-axis of the tetragonal LBCO lies in the LBCO film plane and is parallel to either $[100]_{MgO}$ or $[010]_{MgO}$. The lattice misfit is estimated to be 8% from the high-order electron diffraction spots (Figure 2c). This result, in good agreement with the corresponding value from the XRD data (namely, 7.5% from the lattice parameters of the LBCO and MgO unit cells), suggests that the strain is fully relaxed in the as-grown films. The HREM image of Figure 2d reveals that the as-grown LBCO film has excellent epitaxial character with an atomically sharp and flat surface. It is surprising that the LBCO film can have excellent epitaxial quality, even with a lattice misfit as large as 8%. Neither a precipitate nor any other phase was present in the film or at the interface. However, plenty of edge dislocations are formed over the entire interface (see below).

Figure 2e shows a plan-view HREM image of a LBCO film exhibiting orthogonal nanopattern structures (called nanodomains hereafter) consisting of perpendicular edges with dimensions of several nanometers (~2−10 nm) and a sharp domain boundary width of ~2 Å. The *c*-axis of the tetragonal LBCO in some nanodomains is perpendicular to that in the other nanodomains, forming 90° rotated domains. The electron diffraction pattern taken from a large nanodomain of Figure 2e (see the inset) indicates that the film has excellent single crystallinity. In addition, the weak diffraction spots located at the midpoints between two adjacent strong spots indicate the formation of the 112-type ordered tetragonal structure in the LBCO film. The *c*-axis of the tetragonal LBCO lies in the LBCO film plane and is parallel to either $[100]_{MgO}$ or $[010]_{MgO}$. Thus, the weak diffraction patterns may indicate either the nanoscale ordered tetragonal structure arising from the A-site ordering,[17,18] or the structure associated with the oxygen vacancy ordering, or a combination of the two.

Magnetic and Electrical Transport Properties. Magnetization measurements were conducted to probe the physical properties of the films before and after annealing under oxygen. Figure 3a shows that both oxygen-annealed and as-grown LBCO films exhibit spontaneous magnetizations *M* below ~170 K, which is slightly lower than that reported for the bulk material.[18] This difference could arise from the intrinsic strain and/or crystal defects in the epitaxial films. The spontaneous magnetization follows the scaling law $M \propto (T_c - T)^{\alpha}$ with $\alpha = 0.42 \pm 0.02$ and $T_c = 165$ K, indicating a behavior that falls between that of two- and three-dimensional ferromagnets. The negative magnetization observed at low temperatures (40 and 10 K) may result from the suppression of the spin fluctuations from the nanodomain boundaries, similar to that reported for the $(La,Sr)CoO_3$ thin films.[22,23]

The electrical resistivities of the LBCO films in the temperature range of 10−295 K are shown in Figure 3b. The resistivities of both the annealed and as-grown films increase exponentially with decreasing temperature, indicating the LBCO films to be semiconductors. However, the resistivity for the oxygen annealed film shows a semimetallic behavior below 50 K (Figure 3b). The inset of Figure 3b shows the MR as a function of applied magnetic field measured from 0 T to 7 T and then from 7 T back to 0 T, obtained by using isothermal MR measurements. Here,

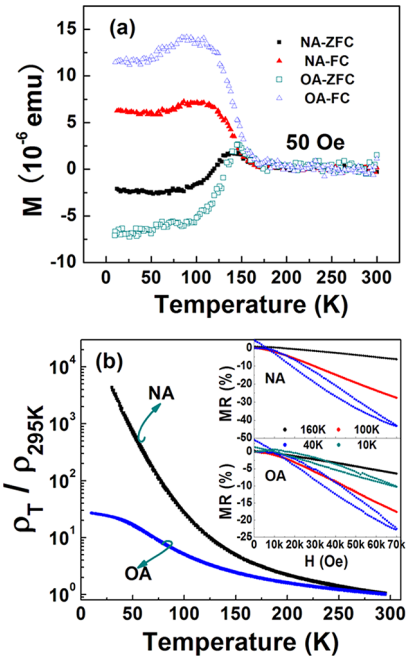

Figure 3. Temperature dependence of the magnetizations and electrical resistivities of the oxygen-annealed (OA) and as-grown, i.e., not annealed (NA), LBCO films grown on (001) MgO: (a) field-cooled (FC) and zero-field-cooled (ZFC) magnetizations measured for the LBCO films; (b) electrical resistivities of the LBCO films, where the inset shows the MR determined as a function of applied magnetic field by isothermal MR measurements.

$$\mathrm{MR}\,(\%) = \frac{\rho(7) - \rho(0)}{\rho(0)} \times 100$$

where $\rho(7)$ and $\rho(0)$ are the resistivities measured at 7 and 0 T, respectively. The MR values are greater for the as-grown than for the oxygen-annealed films. An unusually large MR of ~43% is obtained at 40 K, which is much greater than the MR of the LBCO films grown on $SrTiO_3$ (19% at 40 K)[21] or any phase of the bulk LBCO materials (the large MR value of 14% at 10 K is from the A-order site phase).[17] However, the saturated moments m_s of the annealed samples are much larger than those of the as-grown samples (see Figure 3a).

Figures 4a and 4b show the magnetic hysteresis loops measured for the annealed and as-grown films at various temperatures. The hysteresis loops are symmetrical at temperatures higher than ~100 K, but become unsymmetrical at lower temperatures. At 30 K, the unsymmetrical coercive fields are 13 and −2782 Oe for the as-grown films, and 96 and −485 Oe for the annealed films. For both the annealed and as-grown films, the coercive fields are 275 and −270 Oe at 100 K with the saturation moments reaching the maximum values of 4.46×10^{-5} and 9.43×10^{-5} emu, respectively. To further characterize the magnetic properties of the LBCO films, the magnetic hysteresis loops were measured at 30 K at different magnetic field scan widths at 30 K (see Figures 4c and 4d). The hysteresis loops are unsymmetrical in low-field scans, but become more symmetrical in high-field scans (i.e., higher than 1 T). It is interesting to note that, in the field scans for both annealed and unannealed films, the scan loops do not change upon decreasing the field but do upon increasing the field. This

dx.doi.org/10.1021/am301427c | ACS Appl. Mater. Interfaces 2012, 4, 5524−5528

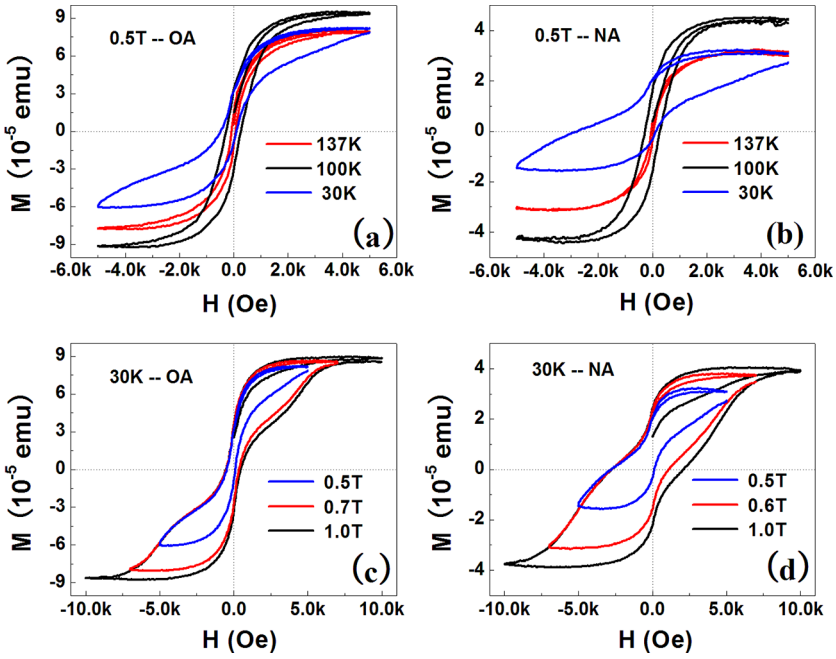

Figure 4. Magnetic hysteresis of the as-grown and oxygen-annealed LBCO films grown on (001) MgO: (a, b) the dependence of the hysteresis loops on temperature measured with the field scan width (−0.5 T to +0.5 T); (c, d) the dependence of the hysteresis on the field scan width measured at 30 K.

phenomenon suggests that the ferromagnetic domains are somewhat clamped at the interfaces between the films and substrates, similar to the results found for the ferroelectric thin films.[24] Furthermore, at 1 T, the coercive fields are −2752 and 2125 Oes for the as-grown films, and −485 and 500 Oes for the annealed films. The large coercive field of the as-grown film indicates that it consists of nanoscale ordered $LaBaCo_2O_{5.5+\delta}$ phases, and the lower coercive field of the oxygen annealed film suggests that the ordered $LaBaCo_2O_{5.5+\delta}$ phases have larger domain sizes.[15] It is most likely that the unsymmetrical hysteresis loop are related to the clamped magnetic polarization at the interface under strong strain or magnetostriction. In fact, the interface strain layer can be clearly seen in the cross-sectional TEM image (the dark layer near the interface in Figure 2a). Thus, at low temperature (<80 K), the large interface strain from the large lattice mismatch between the LBCO film and MgO substrate will result in the clamped-domain formation. The polarization change in such clamped domains can only be achieved at higher magnetic field or at higher temperature.

To further understand the clamped domain effect on the magnetic property, especially the anisotropic magnetic properties of LBCO thin film, we measured the dependence of the resistance of a sample film on the orientation of its plane with respect to the magnetic field direction, as summarized in Figure 5a, where the orientation angles of 0° and 90° mean that the magnetic field is perpendicular and parallel to the surface of the film, respectively. Figure 5b shows that, as a function of the orientation angle, the MR value varies from 46% to 54%, with a maximum being observed when the field H is parallel to the c-axis of the LBCO thin film, indicating that the film has strong magnetic anisotropic properties. This anisotropic behavior implies that the Co spins in the interface region of the film have a preferred spin orientation (e.g., parallel to the film plane). The presence of a preferred spin orientation can give rise to a large change in the MR as a function of the film orientation.

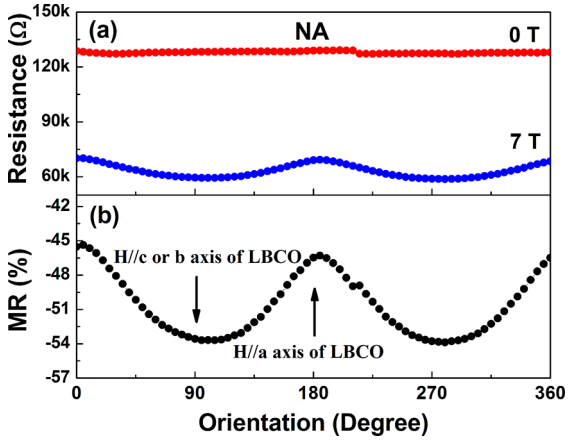

Figure 5. Dependence of the resistivity and the MR of the LBCO thin films on the film orientation, with respect to the magnetic field direction: (a) resistance at 0 T and 7 T and (b) MR at 7 T.

CONCLUSIONS

In summary, highly epitaxial LBCO thin films were successfully grown on the (001) MgO substrates by pulsed-laser deposition. Microstructural characterizations by X-ray diffraction (XRD) and transmission electron microscopy (TEM) show that the LBCO films are a-axis-oriented with an atomically sharp interface. The in-plane interface relationships between LBCO film and MgO substrate have been given by $(100)_{LBCO}//(001)_{MgO}$ and $[001]_{LBCO}//[100]_{MgO}$ or $[010]_{MgO}$. The electrical transport and magnetic property measurements reveal that the LBCO films show an ultralarge MR varied from 46% to 54%, as a function of the orientation angles, This anisotropic behavior further implies that the Co spins have a preferred orientation in the interface region of the film. Moreover, anomalous magnetic phenomena that have been observed for the LBCO films before and after oxygen annealing are

dx.doi.org/10.1021/am301427c | ACS Appl. Mater. Interfaces 2012, 4, 5524−5528

associated most likely with the clamped domains around the interface between the LBCO films and MgO surfaces.

AUTHOR INFORMATION

Corresponding Author

*E-mail: cl.chen@utsa.edu.

Notes

The authors declare no competing financial interest.

ACKNOWLEDGMENTS

This research was partially supported by the Department of Energy under Award Nos. DE-FE0003780, DE-FG26-07NT43063, and DE-SC0001284, the National Science Foundation under Award No. NSF-NIRT-0709293, the State of Texas through the Texas Center for Superconductivity at the University of Houston, and the Natural Science Foundation of China (under No. 11028409). Also, M.L. and C.R.M. would like to acknowledge the support from the "China Scholarship Council" for their Ph.D. research at UTSA, and A.J.J. acknowledges support from the Robert A Welch Foundation (Grant No. E-0024).

REFERENCES

(1) Qi, T. F.; Korneta, O. B.; Parkin, S.; De Long, L. E.; Schlottmann, P.; Cao, G. *Phys. Rev. Lett.* **2010**, *105*, 177203.

(2) Bao, W.; Mao, Z. Q.; Qu, Z.; Lynn, J. W. *Phys. Rev. Lett.* **2008**, *100*, 247203.

(3) Xiong, G. C.; Li, Q.; Ju, H. L.; Greene, R. L.; Venkantesan, T. *Appl. Phys. Lett.* **1995**, *66*, 1689−1691.

(4) See, for example: Jacobson, A. J. *Chem. Mater.* **2010**, *22*, 660−670.

(5) De Souza, R. A.; Kilner, J. A. *Solid State Ionics* **1998**, *106*, 175−187.

(6) Post, M. L.; Tunney, J. J.; Yang, D.; Du, X.; Singleton, D. L. *Sens. Actuators, B* **1999**, *59*, 190−194.

(7) Wang, D. W; Tunney, J. J.; Du, X.; Singleton, D. L.; Post, M. L.; Gauvin, R. *J. Appl. Phys.* **2008**, *104*, 023530.

(8) Wang, S.; Verma, A.; Yang, Y. L.; Jacobson, A. J.; Abeles, B. *Solid State Ionics* **2001**, *140*, 125−133.

(9) Fauth, F.; Suard, E.; Caignaert, V. *Phys. Rev. B* **2002**, *65*, 060401.

(10) Taskin, A. A.; Lavrov, A. N.; Yoichi, A. *Appl. Phys. Lett.* **2005**, *86*, 091910.

(11) Kim, G.; Wang, S.; Jacobson, A. J.; Chen, C. L.; Reimus, L.; Brodersen, P.; Mims, C. A. *Appl. Phys. Lett.* **2006**, *88*, 024103.

(12) Kim, G.; Wang, S.; Jacobson, A. J.; Reimus, L.; Brodersen, P.; Mims, C. A. *J. Mater. Chem.* **2007**, *17*, 2500−2505.

(13) Yuan, Z.; Liu, J.; Chen, C. L.; Wang, C. H.; Luo, X. G.; Chen, X. H.; Kim, G. T.; Huang, D. X.; Wang, S. S.; Jacobson, A. J.; Donner, W. *Appl. Phys. Lett.* **2007**, *90*, 212111.

(14) Fauth, F.; Suard, E.; Caignaert, V.; Domenges, B.; Mirebeau, I.; Keller, L. *Eur. Phys. J. B* **2001**, *21*, 163−174.

(15) Nakajima, T.; Ichihara, M.; Ueda, Y. *J. Phys. Soc. Jpn.* **2005**, *74*, 1572−1577.

(16) Kundu, A. K.; Rautama, E. L.; Boullay, P.; Caignaert, V.; Pralong, V.; Raveau, B. *Phys. Rev.* **2007**, *76*, 184432.

(17) Rautama, E. L.; Boullay, P.; Kundu, A. K.; Caignaert, V.; Pralong, V.; Karppinen, M.; Raveau, B. *Chem. Mater.* **2008**, *20*, 2742−2750.

(18) Rautama, E. L.; Caignaert, V.; Boullay, P.; Kundu, A. K.; Pralong, V.; Karppinen, M.; Ritter, C.; Raveau, B. *Chem. Mater.* **2009**, *21*, 102−109.

(19) Jiang, X. N.; Wang, S.; Kim, G.; Liu, J.; Liu, M.; Gong, W. Q.; Chen, C. L.; Jacobson, A. J. *Mater. Res. Soc. Symp. Proc.* **2009**, *1126*, 15−20.

(20) Liu, J.; Liu, M.; Collins, G.; Chen, C. L.; Jiang, X. J.; Gong, W. Q.; Jacobson, A. J.; He, J.; Jiang, J. C.; Meletis, E. I. *Chem. Mater.* **2010**, *22*, 799−802.

(21) Liu, M.; Liu, J.; Collins, G.; Ma, C. R.; Chen, C. L.; He, J.; Jiang, J. C.; Meletis, E. I.; Jacobson, A. J.; Zhang, Q. Y. *Appl. Phys. Lett.* **2010**, *96*, 132106.

(22) Luo, G. P.; Wang, Y. S.; Chen, S. Y.; Heilman, A. K.; Chen, C. L.; Chu, C. W.; Liou, Y.; Ming, N. B. *Appl. Phys. Lett.* **2000**, *76*, 1908−1910.

(23) Kwon, C.; Gim, Y.; Fan, Y.; Hundley, M. F.; Roper, J. M.; Arendt, P. N.; Jia, Q. X. *Appl. Phys. Lett.* **1998**, *73*, 695−697.

(24) Liu, M.; Collins, G.; Silva, E.; Ma, C. R.; Liu, J.; Chen, C. L.; He, J; Jiang, J. C.; Meletis, E. I.; Qu, S. W.; Zhang, Q. Y.; Bhalla, A. *Integr. Ferroelectr.* **2011**, *131*, 89−94.

NOTE ADDED AFTER ASAP PUBLICATION

This paper was published on the Web on September 21, 2012. This paper was intended not to have Supporting Information. The SI was removed and the corrected version was reposted on September 24, 2012.